IEEE Access
Multidisciplinary | Rapid Review | Open Access Journal

Received February 24, 2019, accepted March 11, 2019, date of publication March 18, 2019, date of current version November 12, 2019.

Digital Object Identifier 10.1109/ACCESS.2019.2905656

Wavefront Control of 2D Curved Coding Metasurfaces Based on Extended Array Theory

YANG ZHOU[1], JIANLIANG XIE[1], HAIYAN CHEN[1], LI ZHANG[1], YAO YAN[2], FENGXIA LI[1], LINBO ZHANG[1], PEIHENG ZHOU[1], (Member, IEEE), AND LONGJIANG DENG[1]

[1]National Engineering Research Center of Electromagnetic Radiation Control Materials, Key Laboratory of Multi-Spectral Absorbing Materials and Structures of Ministry of Education, State Key Laboratory of Electronic Thin Films and Integrated Devices, University of Electronic Science and Technology of China, Chengdu 610054, China
[2]Department of Development and Planning, North Automatic Control Technology Institute, Taiyuan 030000, China

Corresponding author: Haiyan Chen (chenhy@uestc.edu.cn)

This work was supported in part by the National Natural Science Foundation of China under Grant 61471097 and Grant 51772042, in part by the 111 Center under Grant B13042, and in part by the Program for Changjiang Scholars and Innovative Research Team in University (PCSIRT).

ABSTRACT We extend the array theory to design 2D curved coding metasurfaces in order to achieve arbitrary wavefront control. The extended array theory establishes the relationship between wavefront and curved-surface, which provides a simple and effective method to obtain the layout of desired metasurfaces. According the theory, we present 2D curved metasurfaces with 3-bit coding elements. Both simulations and measurements demonstrate that the proposed designs can manipulate wavefront effectively. For normal incidence, the aperture efficiency of normal reflection is more than 90%. For general oblique incidence, the proposed designs almost meet the expectances, but the aperture efficiency decreases with the increase of desired scattering elevation angle. The curved coding metasurfaces are expected to be applied to many devices such as conformal antenna array.

INDEX TERMS Curved metasurfaces, wavefront control, array theory, coding metasurfaces.

I. INTRODUCTION

Metasurfaces, two-dimensional (2D) counterparts of three-dimensional (3D) metamaterials, are periodic or quasi-periodic ultrathin planar artificial structure with sub-wavelength elements arranged in special rules. In 2011, Capasso et al. proposed the Generalized Snell's law [1], which depicts the basic electromagnetic (EM) properties of metasurfaces. When the EM wave is reflected or transmitted on metasurfaces, discontinuous phase and amplitude shifts will be introduced due to the resonances of subwavelength elements, which lead to the anomalous reflection or refraction. By designing the desired array layouts, with desired phase and amplitude of elements, a plethora of metasurface devices, such as anomalous scattering [2], [3], invisible cloak [4]–[6], polarizers [7] and holographic imagers [8], [9] have been created.

Many planar metasurfaces for controlling wavefront have been studied based on traditional array theory, which is used in planar lens [10], [11], antenna array [12] and RCS (Radar cross section) reduction [13]–[16] in this method. In 2007, Paquay used array theory to describe the RCS reduction of checkerboard-like AMC (Artificial magnetic conductor) structure [17]. The array theory can calculate the far-field information of metasurfaces through the distribution of their cells. In 2014, Cui et al. put forward the concept of coding metasurfaces [18], and used array theory to analyze and design planar coding metasurfaces. Due to the digital properties of "0" and "1" elements, coding metasurfaces is easy to combine with optimization algorithm and to realize automatic computer design. In recent years, study attention gradually changes from the planar metasurfaces to conformal metasurfaces [19]–[21] due to the applications of conformal

The associate editor coordinating the review of this manuscript and approving it for publication was Kuang Zhang.

antenna array. However, the traditional array theory cannot help quickly design conformal metasurfaces. Design of conformal metasurfaces design requires to establish the relationship between wavefront and curved surface. Therefore, this paper studies on efficiently design 2D curved coding metasurfaces (2D-CCMs) for arbitrary wavefront control, which is expected to be applied to conformal antenna array.

In this work, we proposed the extended array theory to design 2D-CCMs in order to achieve arbitrary wavefront control. Several designs were fabricated, which are flexible metasurfaces backed by metal ground and lay on a metal arc-shaped frame with a central angle of 120°. The metasurfaces consist of a silicone rubber substrate and a top pattern layer that construct by 3-bit coding cells with varying copper polygon. Due to the symmetry of cells, the proposed metasurface is basically polarization-independent. For the normal reflection design at 10 GHz under normal incidence, both simulated and measured results demonstrate the validity, and the aperture efficiency of both polarizations is more than 90%. Extruding or stretching the arc-shaped frame from 110° to 140°, the aperture efficiency of both polarizations is still over 75%. For oblique reflection, 9 different prototypes were designed and simulated, showing the aperture efficiency decreases with the increase of desired reflection elevation angle. When the prototypes are under oblique incidence, it proves the method can also control wavefront in a good performance.

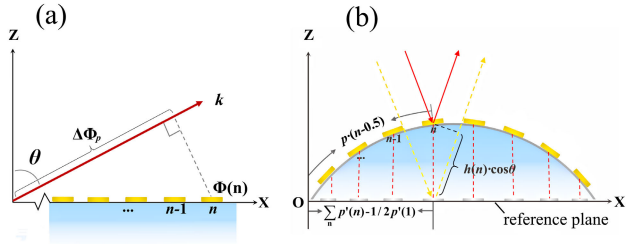

FIGURE 1. (a) The schematic of n-order 1D planar metasurfaces, where red arrow shows free-space vector k and $\Delta\Phi_p$ is the projection of lattices position in the direction θ. (b) The schematic of 2D curved metasurface and equivalent planar metasurface, which shows the relation between 2D curved-surface and reference plane.

A. EXTENDED ARRAY THEORY

We started far-field analysis with 1D planar metasurfaces. Here, a metasurface with period p is placed in the XOZ plane, as shown in Fig. 1a. We assumed that all the elements in metasurface have the equal reflection amplitude of 1. According to the traditional array theory, the scattering pattern at any elevation angle θ can be expressed as:

$$f(\theta) = \sum_n e^{-i[\Phi(n)+\Delta\Phi_p]}, \Delta\Phi_p = k_0 p \sin\theta \cdot (n - 0.5) \quad (1)$$

where k_0 is the wave vector in free space. In the *n-th* lattice, a discontinuous phase shift $\Phi(n)$ has been introduced. Note that $\Delta\Phi_p$ indicates the scattering phase affected by lattice position. Because we regarded the central of sub-wavelength cells as reference points, the distance from *n-th* lattice to origin is $p\cdot(n\text{-}0.5)$, which depends on the selection of reference point. Obviously, the total scattering pattern is easy to calculate by adding up all the patterns of each lattice. However, (1) cannot be applied to oblique incidence, due to the ignorance of the phase shift introduced by incident direction. Therefore, the phase response $\Delta\Phi_i$ caused by oblique incidence need to be considered, which derivation is similar to $\Delta\Phi_p$. Then, we toke θ_i and φ_i into consideration, and the function could be modified as:

$$\begin{aligned} f(\theta) &= \sum_n e^{-i[\Phi(n)+\Delta\Phi_p+\Delta\Phi_i]}, \\ \Delta\Phi_p &= k_0 p \sin\theta \cdot (n - 0.5), \\ \Delta\Phi_i &= k_0 p \sin\theta_i (n - 0.5) \end{aligned} \quad (2)$$

In order to extend the function to 2D-CCMs, an equivalent planar metasurface was assumed to simplify the analysis process, as shown in Fig. 1b. Then, the RCS pattern of 2D-CCMs can be rewritten as:

$$\begin{aligned} f(\theta) &= \sum_n e^{-i[\Phi(n)+\Delta\Phi'_p+\Delta\Phi'_i+\Delta\Phi_h]}, \\ \Delta\Phi_h &= 2kh(n)\cos\theta_i - \pi, \\ \Delta\Phi'_p &= k_0 \sin\theta \cdot \sum_n p'(n) - 0.5p'(1), \\ \Delta\Phi'_i &= k_0 \sin\theta_i \cdot \sum_n p'(n) - 0.5p'(1) \end{aligned} \quad (3)$$

$\Delta\Phi_h$ shows the phase difference between curved surface and reference plane. Apparently, the equivalent planar metasurface has varying lengths of lattices $p'(n)$, which is the projection of lattices on reference plane. Therefore, the expressions of $\Delta\Phi\prime_p$ and $\Delta\Phi'_i$ will change based on the equivalent planar metasurface. Similarly, under arbitrary incidence (θ_i, φ_i) in upper space, the far field of 2D-CCMs in arbitrary direction (θ, φ) can be derived as:

$$\begin{aligned} f(\theta,\varphi) &= \sum_n e^{-i[\Phi(n,m)+\Delta\Phi'_p+\Delta\Phi'_i+\Delta\Phi_h]} \\ \Delta\Phi_h &= 2kh(n,m)\cos\theta_i - \pi \\ \Delta\Phi'_p &= k_0 \sin\theta \cdot [\cos\varphi \sum_n p'(n) - 0.5p'(1) \\ &\quad + \sin\varphi \sum_m q'(m) - 0.5q'(1)] \\ \Delta\Phi'_i &= k_0 \sin\theta_i \cdot [\cos\varphi_i \sum_n p'(n) - 0.5p'(1) \\ &\quad + \sin\varphi_i \sum_m q'(m) - 0.5q'(1)] \end{aligned} \quad (4)$$

As shown in (4), the variation φ is azimuth angle, while n and m are the sequence of lattices along x-axis and y-axis. From the above equations, we clearly observe the manipulation of scattering pattern by encoding metasurface lattices, which is helpful for designing 2D curved metasurfaces under arbitrary incidence. Combining with the global optimization, it can automatically obtain various reasonable designs via computer.

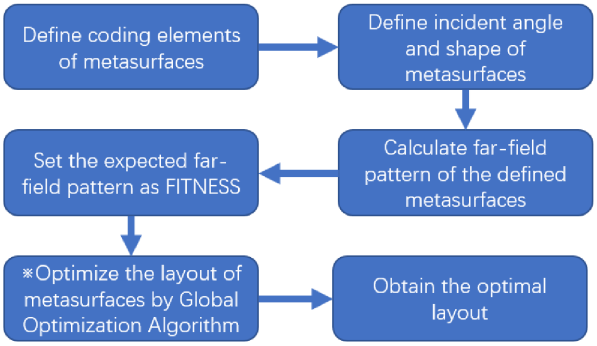

FIGURE 2. Flowchart of design process.

TABLE 1. The parameters of 3-bit coding sub-wavelength elements.

No.	000	001	010	011	100	101	110	111
d	7.4	7.2	6.9	6.6	6.6	6.8	5.9	4.6
g	0	1.4	1.1	0.2	0.8	1.8	0.3	2.3
phase	-160°	-115°	-70°	-25°	20°	65°	110°	155°

II. WAWEFRONT CONTROL

A. NORMAL REFLECTION DESIGN

An arc-shaped coding metasurface was designed to demonstrate the validity of extended array theory. Generally, the reflection of arc structures is different from that of plane structures. Arc structures diffuse EM waves to all directions rather than normal direction. The diffusion is determined by the shape of structures, including curvature radius and central angle. According to the extended array theory, we designed an arc-shaped metasurface and coated it on arc-shaped frame, which expects to achieve normal reflection under 10 GHz normal incidence. The flowchart of design process is shown in Fig. 2, where the step with star label has been reported in our previous work [16].

The elements of arc-shaped metasurface are sub-wavelength sandwich structures with a periodic of $p = 7.5$ mm, as shown in Fig. 3a. The substrate is silicone rubber with a thickness of h = 1 mm and the permittivity is $\varepsilon = 3.3$, $tg\delta = 0.01$. The top layer is copper polygon pattern, whose reflection phase varies with the parameters d and g. Therefore, we chose 3-bit coding elements numbered from '000' to '111', which are marked in Fig. 3b. Their detailed parameters and reflection phase are list in Table 1.

The arc-shaped metasurface has an array of 40×40, and the total length is 300 mm. The central angle of arc is 120° and its curvature radius is 144 mm. In order to observe the performance of normal reflection, we simulated the RCS pattern of the arc-shaped metasurface and bare arc-shaped frame, as shown in Fig. 4. Due to central symmetry of polygon pattern, the arc-shaped metasurface is polarization independence. In this paper, x-polarization is defined as electric field along the x-axis, and y-polarization is defined as electric field along the y-axis. As shown in Fig. 4, the RCS patterns are normal reflection with a amplitude of 17.2 dBsm for y-polarization and 17.8 dBsm for x-polarization, respectively.

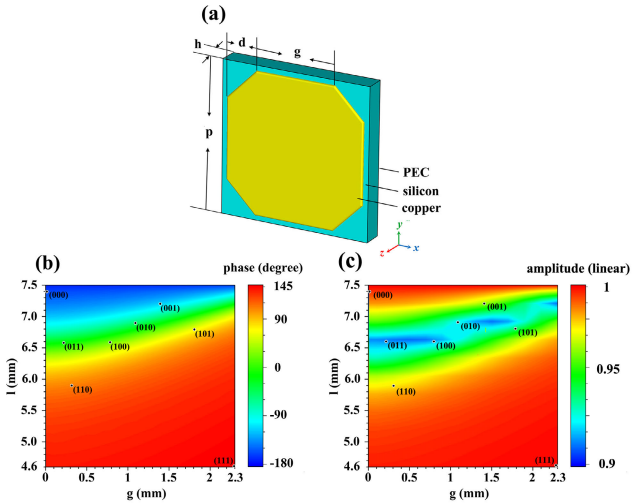

FIGURE 3. (a) Schematic of polygon cells with varying d and g, which thickness $h = 1$ mm and period $p = 7.5$ mm. (b) Simulation of reflection phases and (c) amplitudes of polygon cells at 10GHz versus parameter d and g. The selections of 3-bit elements are labelled on the diagram.

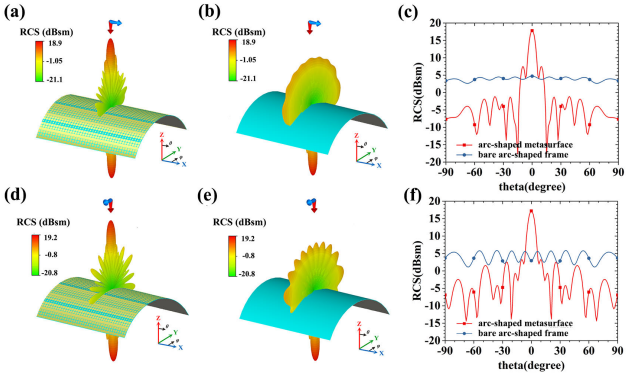

FIGURE 4. RCS patterns of x-polarization waves with a frequency of 10 GHz at normal incidence for (a) arc-shaped metasurface and (b) arc-shaped bare frame. (c) Bistatic RCS in YOZ plane under $x-$ polarization. RCS patterns of $y-$ polarization waves with a frequency of 10 GHz at normal incidence for (d) arc-shaped metasurface and (e) arc-shaped bare frame. (f) Bistatic RCS in YOZ plane under y-polarization.

In addition, it is obvious that y-polarization excites higher side lobes in YOZ plane, resulting in a slightly lower main lobe than x-polarization.

According to antenna theory, aperture efficiency $\eta\alpha$ is defined as the ratio of two main lobe of reflection [22]:

$$\eta_\alpha = \frac{R_m}{R_{\text{ae}}} \tag{5}$$

R_m is the reflection of arc-shaped metasurface, and R_{ae} is the reflection of a metallic plate which occupies the same effective aperture as the arc. Therefore, the aperture efficiency of x-polarization and y-polarization are 94% and 90%, showing a very high efficiency of normal reflection at 10 GHz. For extruding or stretching the arc-shaped frame from 100° to 140°, the arc-shaped metasurface can also achieve high efficient normal reflection. The simulations of aperture efficiency and bistatic RCS of main lobe are shown

TABLE 2. The parameters of 3-bit coding sub-wavelength elements.

Central angle (°)	100	110	120	130	140
x-polarization RCS (dBsm)	7.3	14.3	17.8	17.2	13.6
y-polarization RCS (dBsm)	10.4	15.0	17.2	16.7	13.4
x-polarization aperture efficiency	38.0%	75.3%	95.0%	93.2%	75.1%
y-polarization aperture efficiency	54.0%	79.0%	91.7%	90.7%	74.0%

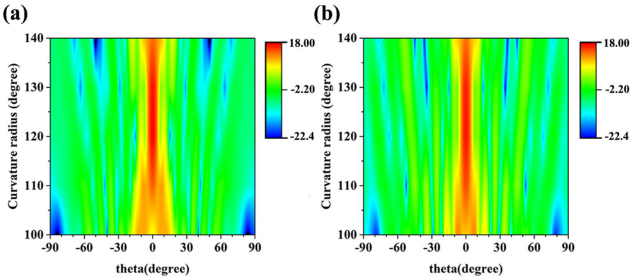

FIGURE 5. Bistatic RCS simulations of arc-shaped metasurfaces with central angles ranging from 100 to 140 under two polarizations normal incidence: (a) *x*- polarization and (b) *y*-polarization.

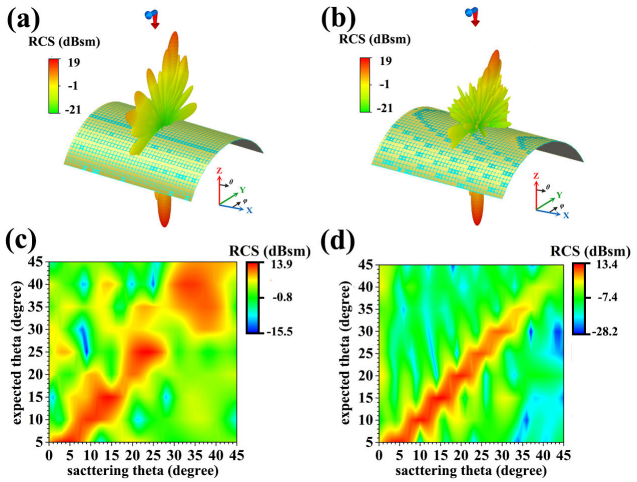

FIGURE 6. RCS patterns of 15° oblique reflection designs that reflect in two normal plane (a) YOZ plane, (b) XOZ plane. And bistatic RCS of (c) YOZ plane and (d) XOZ plane, each graph displays 9 different designs that oblique reflect in every 5° from 5° to 45°.

in Fig. 4. In Fig. 5a-b, *x*-axis displays scattering direction, and *y*-axis represents the different central angle. Obviously, the main lobe gradually splits during the central angle far away from 120°. As shown in Table 2, the aperture efficiency is still larger than 75% from 110° to 140°. Therefore, simulations prove that the designed metasurface is able to achieve high efficient normal reflection, and it is also valid in a wide range of central angles.

B. ARBITRARY REFLECTION DESIGN

Under normal incidence, several different arc-shaped metasurfaces were designed to achieve arbitrary oblique incidence

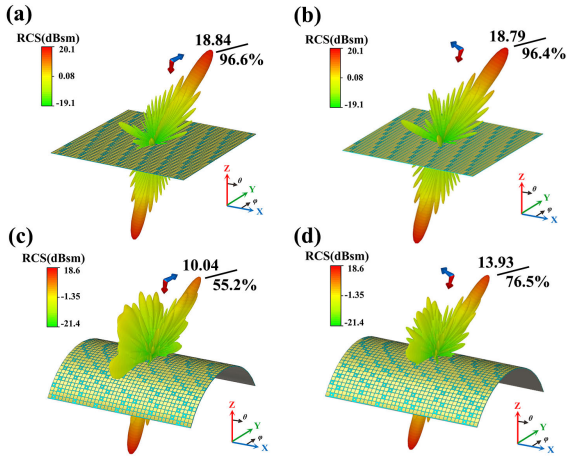

FIGURE 7. RCS pattern simulations of planar and arc-shaped metasurfaces under $(\theta_i, \varphi_i) = (15°, -15°)$ oblique incidence, which amplitudes and aperture efficiencies of main lobes are marked in: (a) planar metasurface under φ-polarization, (b) planar metasurface under θ-polarization, (c) arc-shaped metasurface under φ-polarization, (d) arc-shaped metasurface under θ-polarization.

from 5° to 45°. Fig. 6a and Fig. 6b show the RCS pattern simulations of 15° oblique reflection in YOZ plane and XOZ plane, respectively. Similar to the normal reflection in Fig. 4d-f, under *y*-polarization incidence, there are high sidelobes in YOZ plane, which causes the difficulty of main lobe control, including amplitude and directivity. In Fig. 6c and Fig. 6d, each graph shows the bistatic RCS simulations of 9 different designs that oblique reflect in every 5° from 5° to 45°, where *y*-axis is the expected oblique reflection of design, and *x*-axis is the actual reflection angle. Therefore, the prefect results should display as an obvious diagonal in the diagrams. As shown in Fig. 6c-d, all of the oblique reflection designs are basically satisfied with their expectances. However, due to the high sidelobes in YOZ plane, the 30° design does not meet expectations but scatters to 40°, as shown in Fig. 6c. Due to the sidelobes caused by the parasitic reflections of arc-shaped metasurface [23], the aperture efficiency decreases with the increase of the reflection angle.

In order to verify the validity of oblique incidence, planar and arc-shaped metasurfaces was designed under the incidence of $(\theta_i, \varphi_i) = (15°, -15°)$ at 10 GHz, which is expected to scatter to $(\theta, \varphi) = (30°, 30°)$. The simulations of RCS patterns have been shown in Fig. 7. Note that Cartesian coordinates cannot accurately describe the polarization of oblique incidence, so they were replaced by spherical coordinates. Therefore, Fig. 7a and 7c is under φ-polarization (electric field along φ direction), and Fig. 7b and 7d is under θ-polarization (electric field along θ direction). Obviously, the results show that the main lobes of both planar and arc-shaped metasurfaces point in the expected direction, which indicates the method is valid for oblique incidence. Their amplitudes and aperture efficiencies of main lobes are marked in the graph. For the planar metasurfaces, their main lobes are almost identical and very strong. However, for the arc-shaped

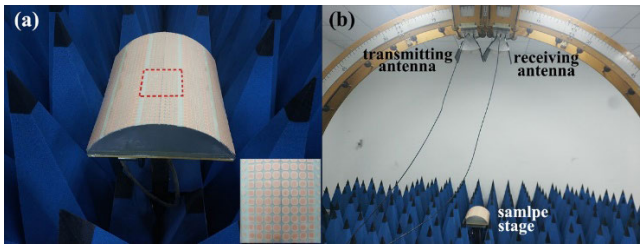

FIGURE 8. (a) Schematic of arc-shaped metasurfaces. The insert shows the local cells distribution. (b) Schematic of microwave test platform.

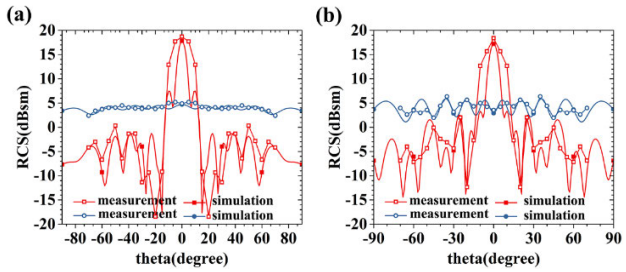

FIGURE 9. Measured and simulated results of bistatic RCS in YOZ plane under (a) x-polarization and (b)y-polarization, where blue line is metallic bare arc-shaped frame and red line is arc-shaped metasurfaces.

metasurfaces, arc-shaped frame generates amounts of side lobes and leads to the lower main lobes. As previous states, a large number of y-component electric field results in the lower main lobe of φ-polarization than θ-polarization.

III. MEASUREMENT

To validate the performance of the proposed arc-shaped metasurfaces, a prototype with 120° central angle was fabricated and measured at 10 GHz. Fig. 8a shows the photograph of fabricated prototype. Its substrate is 1mm flexible silicone rubber laid on metallic arc structure. The polygon patterns of top layer are made of copper-coated polyimide film, which is attached to the flexible silicon substrate by heat transfer method. Fig. 8b shows the experimental setup for the normal incidence. Bistatic RCS is measured by adjusting the elevation of receiving horn antenna, and the polarizations is changed by rotating transmitting and receiving horn antennas simultaneously. The prototype is placed on the sample stage, and a large number of pyramid absorbers surround the stage to eliminate the background reflection.

Fig. 9 shows the measured and simulated results of two polarizations. Obviously, the simulations are in good agreement with the measurements, especially in the normal reflection. The measured main lobe of x-polarization and y-polarization are 18.7 dBsm and 18.3 dBsm, respectively. However, duo to the limitation of test accuracy and prototype accuracy, the main lobe width of measurements is wider than that of simulations, which results in the difference of RCS, especially at the elevation angles between $-20°$ and $+20°$. And the RCS data are measured every 5 degrees, which makes test curves not smooth. When the elevation angle of receiving antenna exceeds 70°, the wall-induced echo makes the test data incorrect, so RCS can only be measured between $-70°$ to $+70°$. Fortunately, this does not affect our results.

IV. CONCLUSION

In a summary, the array theory is extended to 2D-CCMs for controlling the wavefront, which build the relationship between wavefront and curved surface. The arc-shaped coding metasurfaces modelled by extended array theory can manipulate wavefront under arbitrary incidence. Due to the symmetry of polygon cells, the proposed metasurfaces are basically polarization-independent. In the case of arc-shaped metasurfaces with a central angle of 120°, both the simulated and measured results demonstrated that it effectively controls wavefront at 10 GHz. Under normal incidence of both polarizations, the aperture efficiency of normal reflection reaches to over 90%. Bending the central angle of arc from 110° to 140°, the aperture efficiency is still more than 75%. The aperture efficiency decreases with the increase of the reflection angle when the wavefront is manipulated to produce oblique reflection, which can be explained as sidelobe caused by the parasitic reflections of arc-shaped metasurfaces. For oblique incidence, the proposed metasurfaces is still proved to be able to arbitrarily control the wavefront. Similarly, due to the strong sidelobes of arc-shaped structure, the aperture efficiency of both polarizations is about 55% and 76% respectively. Therefore, the curved coding metasurfaces are expected to be employed in many applications such as conformal antenna array. In addition, although we only demonstrate the validity of wavefront control of 2D-CCMs, the extended array theory can also be applied to 3D curved-metasurfaces.

REFERENCES

[1] N. Yu, P. Genevet, M. A. Kats, F. Aieta, J. P. Tetienne, F. Capasso, and Z. Gaburro, "Light propagation with phase discontinuities: Generalized laws of reflection and refraction," *Science*, vol. 334, no. 6054, pp. 333–337, Oct. 2011.

[2] S. Sun, Q. He, S. Xiao, Q. Xu, X. Li, and L. Zhou, "Gradient-index metasurfaces as a bridge linking propagating waves and surface waves," *Nature Mater.*, vol. 11, no. 5, pp. 426–431, 2012.

[3] S. Sun, K.-Y. Yang, C.-M. Wang, T.-K. Juan, W. T. Chen, C. Y. Liao, Q. He, S. Xiao, W.-T. Kung, G.-Y. Guo, L. Zhou, and D. P. Tsai, "High-efficiency broadband anomalous reflection by gradient meta-surfaces," *Nano Lett.*, vol. 12, no. 12, pp. 6223–6229, 2012.

[4] D. Schurig, J. J. Mock, B. J. Justice, S. A. Cummer, J. B. Pendry, A. F. Starr, and D. R. Smith, "Metamaterial electromagnetic cloak at microwave frequencies," *Science*, vol. 314, no. 5801, pp. 977–980, Nov. 2006.

[5] J. B. Pendry, D. Schurig, and D. R. Smith, "Controlling electromagnetic fields," *Science*, vol. 312, pp. 1780–1782, Jun. 2006.

[6] T. Ergin, N. Stenger, P. Brenner, J. B. Pendry, and M. Wegener, "Three-dimensional invisibility cloak at optical wavelengths," *Science*, vol. 328, no. 5976, pp. 337–339, Apr. 2010.

[7] N. Yu, F. Aieta, P. Genevet, M. A. Kats, Z. Gaburro, and F. Capasso, "A broadband, background-free quarter-wave plate based on plasmonic metasurfaces," *Nano Lett.*, vol. 12, no. 12, pp. 6328–6333, Nov. 2012.

[8] L. Huang, X. Chen, H. Mühlenbernd, H. Zhang, S. Chen, B. Bai, Q. Tan, G. Jin, K.-W. Cheah, C.-W. Qiu, J. Li, T. Zentgraf, and S. Zhang, "Three-dimensional optical holography using a plasmonic metasurface," *Nature Commun.*, vol. 4, Nov. 2013, Art. no. 2808.
[9] X. Ni, A. V. Kildishev, and V. M. Shalaev, "Metasurface holograms for visible light," *Nature Commun.*, vol. 4, Nov. 2013, Art. no. 2807.
[10] X. Li, S. Xiao, B. Cai, Q. He, T. J. Cui, and L. Zhou, "Flat metasurfaces to focus electromagnetic waves in reflection geometry," *Opt. Lett.*, vol. 37, no. 23, pp. 4940–4942, Dec. 2012.
[11] F. Aieta, P. Genevet, M. A. Kats, N. Yu, R. Blanchard, and Z. Gaburro, "Aberration-free ultrathin flat lenses and axicons at telecom wavelengths based on plasmonic metasurfaces," *Nano Lett.*, vol. 12, no. 9, pp. 4932–4936, Aug. 2012.
[12] K. Lindfors, D. Dregely, M. Lippitz, N. Engheta, M. Totzeck, and H. Giessen, "Imaging and steering unidirectional emission from nanoantenna array metasurfaces," *ACS Photon.*, vol. 3, no. 2, pp. 286–292, Jan. 2016.
[13] K. Wang, J. Zhao, Q. Cheng, D. S. Dong, and T. J. Cui, "Broadband and broad-angle low-scattering metasurface based on hybrid optimization algorithm," *Sci. Rep.*, vol. 4, Aug. 2014, Art. no. 5935.
[14] Y. Zhao, X. Cao, J. Gao, Y. Sun, H. Yang, X. Liu, Y. Zhou, T. Han, and W. Chen, "Broadband diffusion metasurface based on a single anisotropic element and optimized by the simulated annealing algorithm," *Sci. Rep.*, vol. 6, Apr. 2016, Art. no. 23896.
[15] L. Pulido-Mancera, T. Fromenteze, T. Sleasman, M. Boyarsky, M. F. Imani, M. Reynolds, and D. Smith, "Application of range migration algorithms to imaging with a dynamic metasurface antenna," *J. Opt. Soc. Amer. B, Opt. Phys.*, vol. 33, no. 10, pp. 2082–2092, Oct. 2016.
[16] Y. Zhou, G. Zhang, H. Chen, P. Zhou, X. Wang, L. Zhang, L. Zhang, J. Xie, and L. Deng "Design of phase gradient coding metasurfaces for broadband wave modulating," *Sci. Rep.*, vol. 8, Jun. 2018, Art. no. 8672.
[17] M. Paquay, J. C. Iriarte, I. Ederra, R. Gonzalo, and P. D. Maagt, "Thin AMC structure for radar cross-section reduction," *IEEE Trans. Antennas Propag.*, vol. 55, no. 12, pp. 3630–3638, Dec. 2007.
[18] T. J. Cui, M. Q. Qi, X. Wan, J. Zhao, and Q. Cheng, "Coding metamaterials, digital metamaterials and programmable metamaterials," *Light Sci. Appl.*, vol. 3, p. e218, Oct. 2014.
[19] Y. R. Padooru, A. B. Yakovlev, P.-Y. Chen, and A. Alù, "Line-source excitation of realistic conformal metasurface cloaks," *J. Appl. Phys.*, vol. 112, Oct. 2012, Art. no. 104902.
[20] J. Cheng, S. Jafar-Zanjani, and H. Mosallaei, "All-dielectric ultrathin conformal metasurfaces: Lensing and cloaking applications at 532 nm wavelength," *Sci. Rep.*, vol. 6, Dec. 2016, Art. no. 38440.
[21] S. M. Kamali, A. Arbabi, E. Arbabi, Y. Horie, and A. Faraon, "Decoupling optical function and geometrical form using conformal flexible dielectric metasurfaces," *Nature Commun.*, vol. 7, May 2016, Art. no. 11618.
[22] A. M. H. Wong, P. Christian, and G. V. Eleftheriades, "Binary huygens' metasurfaces: Experimental demonstration of simple and efficient near-grazing retroreflectors for TE and TM polarizations," *IEEE Trans. Antennas Propag.*, vol. 66, no. 6, pp. 2892–2903, Jun. 2018.
[23] A. Díaz-Rubio, V. S. Asadchy, A. Elsakka, and S. A. Tretyakov, "From the generalized reflection law to the realization of perfect anomalous reflectors," *Sci. Adv.*, vol. 3, no. 8, Aug. 2017, Art. no. e1602714.

YANG ZHOU was born in Liaoning, China, in 1989. He received the B.S. degree in electronic science and technology from the University of Electronic Science and Technology of China, Chengdu, China, in 2012, where he is currently pursuing the Ph.D. degree.

His recent research activities include the numerical modeling of novel metamaterials and their applications in wave modulation, antenna arrays, and wave absorber.

JIANLIANG XIE received the Ph.D. degree in material physics and chemistry from the University of Electronic Science and Technology of China (UESTC), Chengdu, China, in 2008.

He has been a Full Professor with the National Engineering Research Center of Electromagnetic Radiation Control Materials, UESTC. His research interests include magnetic materials and devices, functional macromolecules, high-quality adherence systems, and electromagnetic absorbing structure.

HAIYAN CHEN received the Ph.D. degree in microelectronics and solid-state electronics from the University of Electronic Science and Technology of China (UESTC), Chengdu, China, in 2011. In 2015, he received the Chinese Scholarship Council (CSC) Scholarship and pursued study at the Department of Engineering, University of Kentucky, Lexington, KY, USA, as a Visiting Scholar.

Since 2012, he has been with the National Engineering Research Center of Electromagnetic Radiation Control Materials, UESTC, where he is currently an Associate Professor. His research interests include artificial electromagnetic materials, electromagnetic radiation control materials, and particularly study on electromagnetic discontinuous repair materials.

LI ZHANG received the Ph.D. degree in electronic science and technology from the University of Electronic Science and Technology of China, Chengdu, China, in 2012.

She has been with the National Center for Electromagnetic Radiation Control Materials Engineering, University of Electronic Science and Technology of China, where she was promoted to full-time Professor, in 2018. Her research interests include magnetic materials and devices, ultra-high temperature ceramics and coatings, and electromagnetic radiation control materials.

YAO YAN was born in Shanxi, China, in 1989. He received the M.S. degree in material science and engineering from the University of Electronic Science and Technology of China (UESTC), in 2015.

He is currently with the North Automatic Control Technology Institute, Taiyuan, China. His recent research activities include the microwave and radio-frequency circuit design, the numerical modeling of novel metamaterials, and their applications in wave modulation and antenna arrays.

FENGXIA LI received the B.S. degree in electronic information science and technology from Henan Polytechnic University, Jiaozuo, China, in 2015. She is currently pursuing the Ph.D. degree in microelectronics and solid-state electronics with the University of Electronic Science and Technology of China (UESTC), Chengdu, China.

Her recent research interests include the structural design of novel metamaterials and their applications in electromagnetic wave modulation, frequency-selective surfaces, RCS reduction, and wave absorbers.

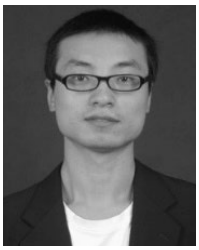

LINBO ZHANG received the Ph.D. degree in microelectronics and solid-state electronics from the University of Electronic Science and Technology of China (UESTC), Chengdu, China, in 2017.

He has been with the National Engineering Research Center of Electromagnetic Radiation Control Materials, UESTC, as an Associate Researcher, since 2017. His research interests include magnetic materials and devices, and electromagnetic absorbing structure.

PEIHENG ZHOU (M'08) received the Ph.D. degree in material physics and chemistry from the University of Electronic Science and Technology of China (UESTC), Chengdu, China, in 2009.

She has been with the State Key Laboratory of Electronic Thin Films and Integrated Devices and the National Engineering Research Center of Electromagnetic Radiation Control Materials, UESTC, where she is currently a Full Professor. Her current research interest includes various aspects of electromagnetic materials or structures, particularly the interplay between electromagnetic wave and materials.

LONGJIANG DENG received the M.S. degree in electronic material and device from the University of Electronic Science and Technology of China (UESTC), Chengdu, China, in 1987.

Since 1987, he has been with UESTC, as a Lecturer, an Associate Professor, and a Full Professor. He has authored/coauthored about 200 articles in refereed international journals and industry publications and given many invited talks in international conferences. His research interests include electromagnetic wave absorbing materials, infrared low emissivity and selective emissivity thin film, and microwave magnetic materials.

Prof. Deng is a member of the Branch of the Chinese Institute of Electronics on Microwave Magnetism, the Vice Director of the Special Committee of the Chinese Institute of Electromagnetic Material, and a member of the Editor Committee of the Chinese *Journal of Functional Materials*.